Metallic stereostructured layer: An approach for broadband polarization state manipulation

Xiang Xiong, Yuan-Sheng Hu, Shang-Chi Jiang, Yu-Hui Hu, Ren-Hao Fan, Guo-Bin Ma, Da-Jun Shu, Ru-Wen Peng, and Mu Wang

Citation: Applied Physics Letters **105**, 201105 (2014); doi: 10.1063/1.4902405
View online: http://dx.doi.org/10.1063/1.4902405
View Table of Contents: http://scitation.aip.org/content/aip/journal/apl/105/20?ver=pdfcov
Published by the AIP Publishing

Metallic stereostructured layer: An approach for broadband polarization state manipulation

Xiang Xiong, Yuan-Sheng Hu, Shang-Chi Jiang, Yu-Hui Hu, Ren-Hao Fan, Guo-Bin Ma, Da-Jun Shu, Ru-Wen Peng, and Mu Wang[a)]
National Laboratory of Solid State Microstructures and Department of Physics, Nanjing University, Nanjing 210093, China

(Received 24 October 2014; accepted 6 November 2014; published online 20 November 2014)

In this letter, we report a full-metallic broadband wave plate assembled by standing metallic L-shaped stereostructures (LSSs). We show that with an array of LSSs, high polarization conversion ratio is achieved within a broad frequency band. Moreover, by rotating the orientation of the array of LSSs, the electric components of the reflection beam in two orthogonal directions and their phase difference can be independently tuned. In this way, all the polarization states on the Poincaré sphere can be realized. As examples, the functionalities of a quarter wave plate and a half wave plate are experimentally demonstrated with both reflection spectra and focal-plane-array imaging. Our designing provides a unique approach in realizing the broadband wave plate to manipulate the polarization state of light.
[http://dx.doi.org/10.1063/1.4902405]

In order to manipulate the polarization state of light, conventionally a wave plate made of a birefringence crystal plate cutting along certain crystallographic orientation is applied.[1] The phase difference between the two orthogonal components of light, usually termed as *o*-ray and *e*-ray, depends on both the birefringence of material and the thickness of the crystal plate. For conventional materials, the available birefringence is usually small (typically 0.1–0.2).[2] To achieve certain phase difference in the two orthogonal directions, the wave plate must be thick enough in order to accumulate the required optical path difference between the *o*- and the *e*-ray. In other words, the geometrical thickness of the crystal plate is the major control parameter of a wave plate. However, as the development of integrated optics and modern on-chip photonics, the spatial size of an optical device becomes extremely limited.[3] In addition, conventional crystalline plate is transparent only for a certain frequency range.[4] It follows that different crystalline material has to be elaborately selected in order to cover a specific frequency band, which further limits the applicability of the optical device based on the birefringence crystalline material. Therefore, it is highly anticipated to design a metastructure that allows people to get rid of the restrictions of the dielectric material in tuning the polarization state of light over a broad frequency range.

In plasmonics developed in recent decade, with certain sub-wavelength metallic microstructures, it is possible to control the polarization of light and achieve various optical properties.[5–13] Most of these optical devices constructed with metallic microstructure have shown interesting optical functionality at a certain frequency range.[13–16] So far, great efforts have been devoted to broaden the response frequency band of the optical device based on metamaterial.[17–21] For example, by superimposing different resonance modes within a unit cell, the bandwidth of the structure can be expanded.[22–25] Besides, metal-insulator-metal structures have been designed by several groups,[5,21] and the behind mechanism[26] has recently been elucidated as the conjugation compensation of the intrinsic dispersion of the metallic structures and the thickness-dependent dispersion of the dielectric spacing layer.

Here, we demonstrate a full-metallic broadband wave plate made of an assembly of standing metallic L-shaped stereostructures (LSSs). As examples, we experimentally demonstrate the functionalities of a quarter wave plate and a half wave plate with the fabricated structure. All the polarization states of light can be achieved within a broad frequency band (over 30% of the center frequency) with this design. In active opto-electric device[27] and display technology,[28] there do exist the circumstances that require a surface acting as an electrode and as a metasurface simultaneously. Therefore, we expect that constructing a stereostructured metallic layer provides a unique approach in designing broadband functional opto-electric devices based on metamaterial.

The array of standing metallic LSSs is fabricated on a glass substrate by two-photon polymerization of UV-curable negative photoresist,[29–31] and details will be described later. A continuous metallic thin film blanket afterwards covers both the polymer standing LSSs and the glass substrate. A sketch of the LSS array and the unit are illustrated in Figs. 1(a) and 1(b), respectively. The coordinate frame is so set that the diagonal directions of LSS unit are defined as x- and y-axes, respectively. The bottom of LSS locates at $z = 0$ as shown in Fig. 1(b). In this way, the two arms of the LSS unit point to 45° and 135°, respectively. The unit cell shown in Fig. 1(b) is reproduced in both 45° and 135° directions, so an array with lattice constant L is constructed. The normal incident light is linearly polarized and propagates in $-z$ and the polarization direction is characterized by angle θ. The finite difference time domain (FDTD) method is applied in calculating the complex amplitude of reflected light. The permittivity of gold in the infrared regime is based on the Drude model $\varepsilon(\omega) = 1 - \omega_p^2 / (\omega^2 + i\omega_\tau\omega)$, where ω_p is the plasma

a)Email: muwang@nju.edu.cn

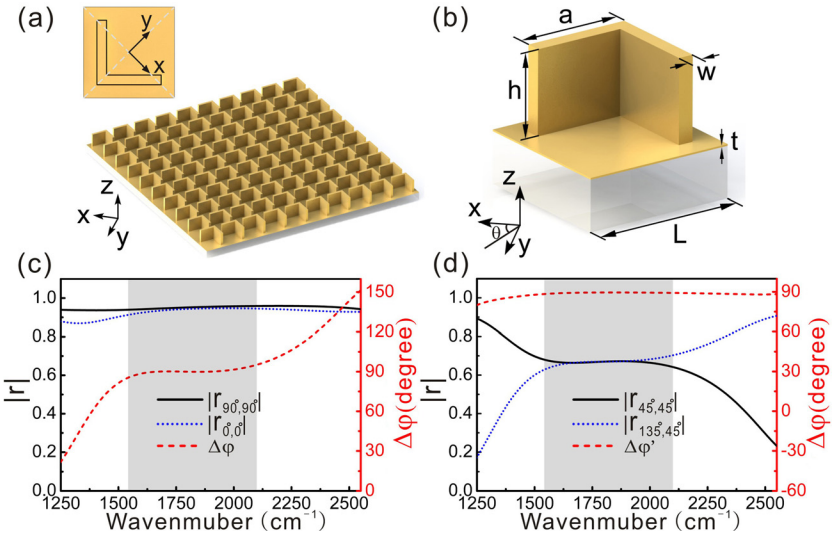

FIG. 1. (a) The schematic diagram of the designing of LSS array. The up left inset shows the top view of the LSS unit. (b) The detailed topography of the designed LSS unit: $L = 3\,\mu$m, $h = 1.7\,\mu$m, $a = 2.1\,\mu$m, $w = 0.3\,\mu$m, and the thickness of the metal film t is 35 nm. θ is the polarization angle. (c) and (d) The calculated amplitudes of reflected light and the phase difference for different polarization arrangements.

frequency and ω_τ is the damping constant. For gold, the characteristic frequencies are taken as $\omega_p = 1.37 \times 10^{16}\,\mathrm{s}^{-1}$ and $\omega_\tau = 1.2 \times 10^{14}\,\mathrm{s}^{-1}$.[32,33] The permittivity of the glass substrate and the L-shaped interior structure is taken as 2.00 and 2.25, respectively.[34]

The incident light is reflected by the LSS array. The amplitude and the phase difference between the two orthogonal components of the reflected light are calculated, as illustrated in Figs. 1(c) and 1(d), respectively, so that the polarization state of the reflected light is fully described. In Figs. 1(c) and 1(d), $r_{m°,n°}$ stands for the complex amplitude of the $m°$-component of reflected light for which the incident light is polarized in $n°$ direction. For the LSS array, the symmetric axes of the structure are in 0° and 90° directions, respectively. When the incident light is polarized in 0° direction (x-direction) or in 90° direction (y-direction), the polarization state of the reflected light remains unchanged. Simulation indicates that the reflectance amplitudes $|r_{0°,0°}|$ and $|r_{90°,90°}|$ are identical and nearly dispersion-free in the range of 1550–2100 cm^{-1}. The phase difference $\Delta\varphi$ between $r_{90°,90°}$ and $r_{0°,0°}$ is 90° in 1550–2100 cm^{-1}. When the polarization of incident light is in 45°, the polarization state of the reflected light will be deviated. The amplitudes of reflectance, $|r_{45°,45°}|$ and $|r_{135°,45°}|$, are identical and are dispersion-free in the range of 1550–2100 cm^{-1}. The phase difference $\Delta\varphi'$ between $r_{45°,45°}$ and $r_{135°,45°}$ is 90° in 1550–2100 cm^{-1}. In this scenario, a right-handed circular polarized (RCP) light is achieved when the incident light is polarized along 45°. Due to the topological symmetry of the LSS unit, when the incident light is polarized along 135°, the reflected light is left-handed circular polarized (LCP). The calculations in Figs. 1(c) and 1(d) indicate that in the frequency range of 1550–2100 cm^{-1}, the LSS array indeed serves as a quarter wave plate, with the fast axis of the LSS quarter wave plate along y-direction (i.e., 90° direction).

We should emphasize that a quarter wave plate constructed with LSS array can realize all the polarization states, which can be illustrated clearly with the Poincaré sphere.[1] On the surface of Poincaré sphere, point $(2\psi, 2\chi)$ represents a state of polarization, where χ is the ellipticity angle as illustrated in the inset of Fig. 2(c) and the angle ψ represents the direction of the major axis of the ellipse polarized light

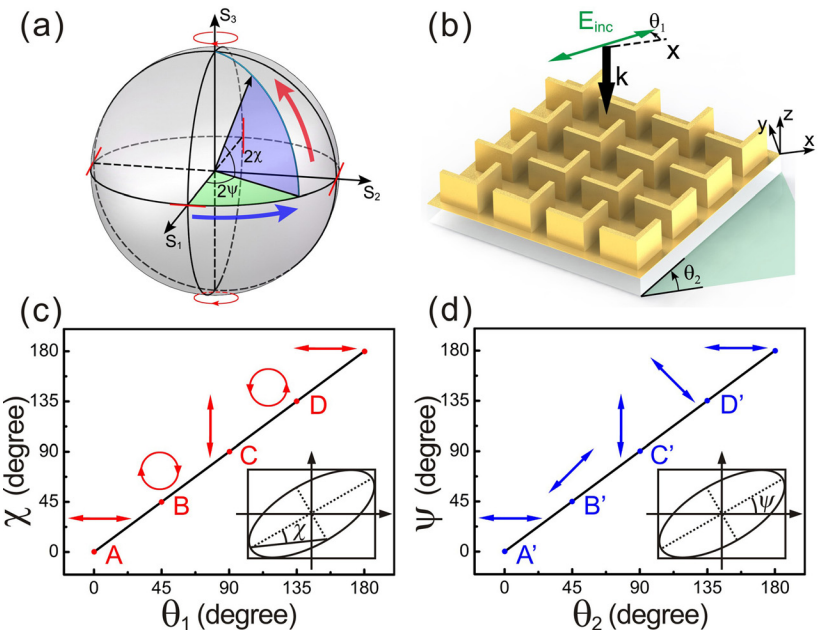

FIG. 2. (a) The schematic micrograph to show the Poincaré sphere. (b) The diagram to show the setup of LSS array. The polarization angle of incident light is θ_1 respected to x-axis, and the whole device is rotated around z-axis for θ_2 angle. (c) The ellipticity angle χ as a function of θ_1. (d)The orientation angle ψ as a function of θ_2.

as shown in the inset of Fig. 2(d). The coordinates S_1, S_2, and S_3 are the normalized Stokes parameters describing the state of polarization. To realize a certain polarization state of light essentially is to find a route to reach a specific point on the surface of Poincaré sphere.

We introduce two independent parameters θ_1 and θ_2 to describe the polarization angle of the incident light and the orientation angle of the LSS array, respectively, as shown in Fig. 2(b). The LSS array locates in the x-y-z Cartesian coordinate. As illustrated in Figs. 1(a) and 1(b), the coordinate frame is so set that the diagonal directions of LSSs are defined as x- and y-directions. The incident light propagates along $-z$-direction. Parameter θ_1 is defined as the angle between x-axis and the polarization of incident light. The incident light $\vec{E}_{inc}$ is projected in x- and y-directions and is expressed as $\vec{E}_{inc}\cos\theta_1\hat{u}_x + \vec{E}_{inc}\sin\theta_1\hat{u}_y$, where $\hat{u}_x$ and $\hat{u}_y$ are the Cartesian unit vectors. As shown in Fig. 1(c), in the frequency range of 1550–2100 cm^{-1}, the phase difference of reflected light in x- and y-directions remains 90°. The amplitude ratio of reflected light in x- and y-directions is $\vec{E}_{inc}\sin\theta_1/\vec{E}_{inc}\cos\theta_1 = \tan\theta_1$. Based on the definition, the ellipticity angle χ is identical to the polarization angle θ_1, i.e., $\chi = \theta_1$. For scenario of $\theta_1 = 0°$, the polarization of the reflected light does not change and its polarization is in 0° direction (Point A in Fig. 2(c)). When θ_1 is increased to 45°, the amplitude ratio between the reflected light in x- and y-directions is $\tan\theta_1 = 1$ and their phase difference is 90°. In this way, a RCP reflected light is realized in 1550–2100 cm^{-1} (Point B in Fig. 2(c)). Similarly, for scenario of $\theta_1 = 90°$ (Point C in Fig. 2(c)), the reflected light is linearly polarized, and the polarization direction is along y-direction. For scenario of $\theta_1 = 135°$, the reflected light is left-circular-polarized (Point D in Fig. 2(c)). If $\theta_1 \neq \frac{n\pi}{4}$ holds (n is integer), the reflected light is elliptically polarized and the principal axes are x and y. Therefore, by rotating the incident polarization to a specific value θ_1, the polarization state of the reflected light may vary from linearly polarized light, circularly polarized light, to elliptically polarized light within a broad frequency range, as shown in Fig. 2(c). In other words, to reach a certain point on the surface of Poincaré sphere, the latitude is controlled by tuning θ_1.

To reach a specific point on the Poincaré sphere, another independent parameter, θ_2, is applied to control the longitude, which is defined as the rotation angle of the LSS array, i.e., the angle that x-y-z Cartesian coordinate rotates around z-axis, as shown in Fig. 2(b). In this scenario, the orientation angle representing the direction of the major axis of the ellipse polarized light ψ equals to θ_2. As illustrated in Fig. 2(d), the orientation angle of the reflected light changes with θ_2. Therefore, θ_1 and θ_2 are the parameters to tune the polarization state of the reflected light. This process can be visualized on the Poincaré sphere. When θ_1 varies while θ_2 is fixed, the polarization state moves along latitude direction, as marked by the red arrow in Fig. 2(a). For the scenario that θ_2 is changed while θ_1 is fixed, the polarization state moves in longitude direction, as indicated by the blue arrow in Fig. 2(a). By rotating the polarization of incident light or rotating the LSS array, any polarization state can be achieved in the reflection beam.

To experimentally verify this expectation, we fabricate the LSS array sample with two-photon polymerization system (Nanoscribe GmbH) on a glass plate (Menzel-Glaser) 170 μm thick. The femtosecond laser beam is focused to a diffraction limited spot, which is then controlled to scan in 3D space to form the LSSs. The exposed negative photoresist (IP-L, Nanoscribe GmbH) is polymerized and generates the backbone of standing L-shaped patterns, while the unexposed photoresist is removed in the developing process. Thereafter, the polymerized L-shaped structures are coated with a homogeneous layer of gold 35 nm in thickness by magnetron sputtering to finalize the metallic stereostructured layer. Figure 3(a) illustrates the field emission scanning electron micrographs (FESEM) of the LSS array, with details shown in Fig. 3(b). Fourier transform infrared (FTIR) spectrometer (Bruker Vertex 70v) is employed to characterize the optical property of LSS array. A pair of ZnSe polarizers is applied to tune the polarization of the incident light and analyze the reflected light. The incident light propagates perpendicularly to the LSS array, with its polarization along 45° direction. The reflectance collected along the polarization direction 0°, 45°, 90°, and 135°, respectively, is illustrated in Fig. 3(c). One may find that when the incident light is polarized in 45°, the amplitude of reflectance $|r_{45°,45°}|$, $|r_{90°,45°}|$, $|r_{135°,45°}|$, and $|r_{0°,45°}|$ is identical and is dispersion-free in the range of 1550–2100 cm^{-1}. When the incident light is polarized in 135°, the amplitude of reflectance $|r_{135°,135°}|$, $|r_{0°,135°}|$, $|r_{45°,135°}|$, and $|r_{90°,135°}|$ shown in Fig. 3(d) is identical and dispersion-free in the range of 1550–2100 cm^{-1} as well. Figure 3(e) illustrates the retrieved $\Delta\varphi_{45°}$ (the phase difference of $r_{45°,45°}$ and $r_{135°,45°}$) and $\Delta\varphi_{135°}$ (the phase

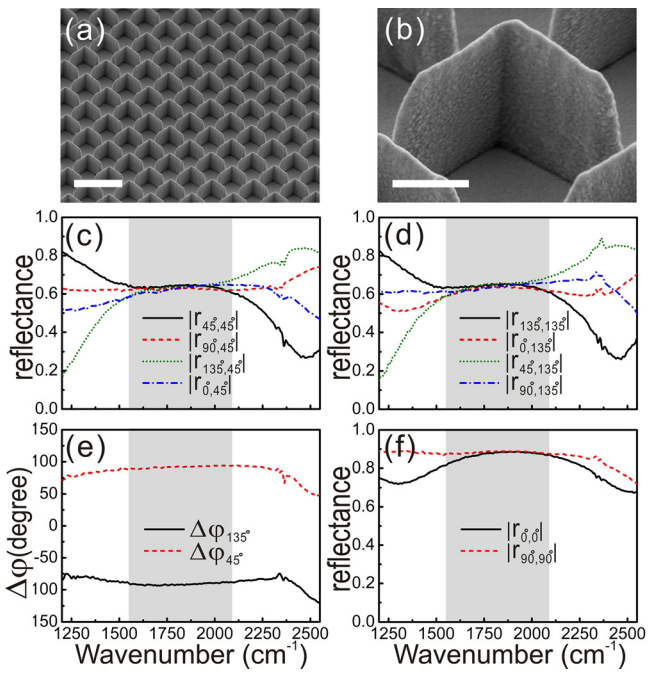

FIG. 3. (a) The FESEM of the fabricated LSS array. The scale bars represent 5 μm. (b) The detailed micrograph of a fabricated LSS unit. The scale bars represent 1 μm. (c) and (d) The measured amplitude of reflectance with four different polarization directions of incidence and reflectance. (e) The phase difference retrieved from the measured amplitudes in (c) and (d). (f) The measured amplitude of reflectance when incident light is along the symmetry axis of the LSS array.

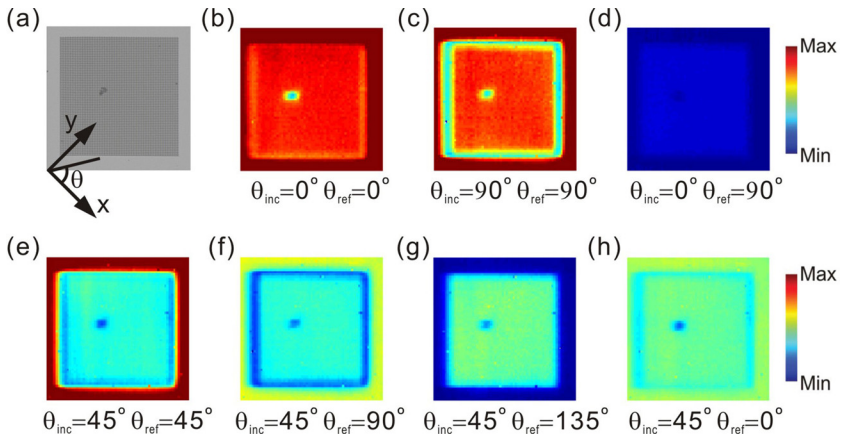

FIG. 4. (a) The optical micrograph of LSS array. *x*- and *y*-directions of the coordinate are set along the diagonal directions of the LSS array. The polarization θ is defined as the angle between the polarization direction and *x*-axis direction. The array is $200\,\mu m \times 200\,\mu m$ in size. In (b)–(h), the incident polarization direction is along θ_{inc} direction, while the reflected signal is collected with a polarizer along θ_{ref} direction.

difference of $r_{135°,135°}$ and $r_{45°,135°}$).[35] One may find that in the range of 1550–2100 cm^{-1}, $\Delta\varphi_{45°} = 90°$ and $\Delta\varphi_{135°} = -90°$. The measured amplitudes and the retrieved phase difference (from measured amplitudes[35]) confirm that a RCP light is achieved when the polarization of incident light is set in 45°. With a similar approach, a LCP light is achieved when the polarization of incident light is set in 135°. We also measure the amplitude of reflected light with the incident light polarized in *x*- and *y*-directions (i.e., 0° and 90°). The measured amplitudes of $r_{0°,0°}$ and $r_{90°,90°}$ are in good agreement with the simulated results shown in Fig. 1(c). Therefore, LSS array works as a quarter wave plate in the frequency range of 1550–2100 cm^{-1}.

To directly demonstrate that LSS array indeed works as a quarter wave plate, focal plane array (FPA) detector (Hyperion 3000, Bruker) is applied to collect the infrared image of the sample. Figure 4(a) shows the topography of the LSS array for FPA measurement. The *x*- and *y*-directions are in two diagonal directions, respectively, as that defined in Fig. 1, and θ is the angle between the polarization direction of incident light and *x*-axis. In Figs. 4(b)–4(h), the FPA image is collected by integrating the signal in 1550–2100 cm^{-1}. The warmer hue indicates that more energy has been collected by the FPA detector. To analysis the polarization state of the reflected light with FPA imaging system, the polarization of incident light is set along θ_{inc} direction. The component in θ_{ref} direction of reflected light is collected by the FPA detector. When the incident light is polarized in the two symmetry directions of the structure (i.e., $\theta_{inc} = 0°$ and 90°), the polarization of the reflected light remains unchanged in 1550–2100 cm^{-1}. This means that no energy is switched to the orthogonal polarization direction. Figures 4(b) and 4(c) correspond to the scenarios that the incident polarization angle is set as $\theta_{inc} = 0°$ and 90°, respectively. Most of energy has been reflected back and collected in the same polarization direction. For this reason, the color of the sample area in Figs. 4(b) and 4(c) is bright red. In Fig. 4(d), the incident polarization ($\theta_{inc} = 0°$) and the collection polarization ($\theta_{ref} = 90°$) are orthogonal. No energy is converted to the orthogonal polarization direction. As a result, the color shown in Fig. 4(d) is dark blue.

In Figs. 4(e)–4(h), the incident polarization is set as $\theta_{inc} = 45°$, and the FPA images are collected with different polarization direction θ_{ref} of the reflected light. The color in the sample areas in Figs. 4(e)–4(h) is nearly identical, suggesting that the reflected light is circularly polarized when the incident direction is set in $\theta_{inc} = 45°$. In Fig. 4(e), the surrounding area is bright red and in Fig. 4(g) the surrounding area is dark blue. This is due to the fact that the polarization of light reflected by the surrounding flat surface remains unchanged.

The broadband optical device with different functionalities can be achieved by tuning the structural parameters of LSS. By setting the lattice constant *L* and the height of LSS *h* as 3.6 μm and 1.4 μm, respectively, a broadband half wave plate can be realized. Figure 5(a) illustrates the fabricated LSSs for half wave plate, and Fig. 5(b) illustrates the detail morphology. Figure 5(c) indicates that the energy of incident light is converted from 45° polarization direction to 135° polarization direction when the incident light is polarized in

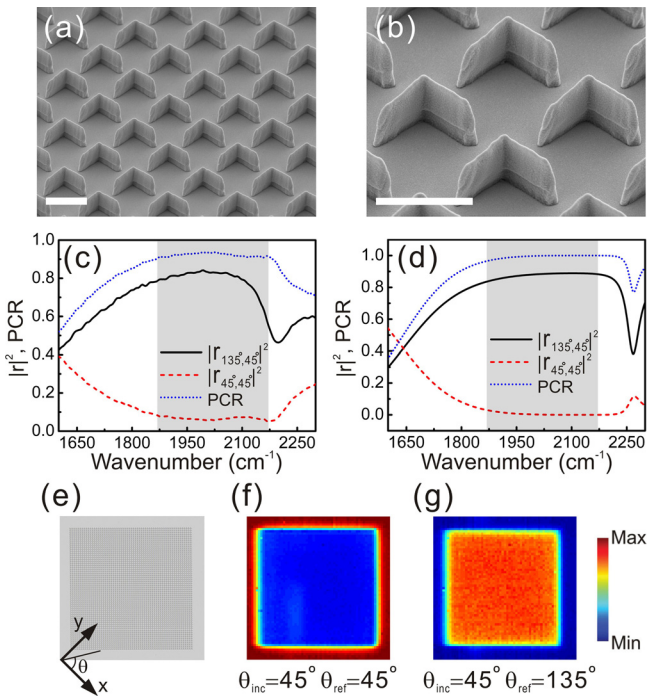

FIG. 5. (a) The FESEM of the half wave plate constructed with LSS array. (b) shows the zoomed in micrograph of the fabricated LSS unit. The scale bars in (a) and (b) represent 3 μm. (c) The measured and (d) calculated results of the reflectivity and PCR of the half wave plate. (e) The optical micrograph of half wave plate. The sample is $200\,\mu m \times 200\,\mu m$ in size. (f) and (g) The FPA images collected with different θ_{inc} and θ_{ref} setup.

45°. Here, the frequency range varies from 1870 cm^{-1} to 2170 cm^{-1}. The polarization conversion ratio (PCR)[14,36] is defined as $PCR = |r_{135°,45°}|^2/(|r_{45°,45°}|^2 + |r_{135°,45°}|^2)$ and the measured PCR is illustrated by the blue dotted line in Fig. 5(c). In 1870–2170 cm^{-1}, PCR is larger than 90%. Simulation shown in Fig. 5(d) further confirms the validity of the measurement.

To verify the spectrum measurement, we apply FPA imaging system and collect the infrared image of LSS with half wave plate feature. The topography of the LSS array is shown in Fig. 5(e), and the FPA images of Figs. 5(f) and 5(g) are integrated from 1870 cm^{-1} to 2170 cm^{-1}. In Fig. 5(f), the incident polarization and the collection polarization are both in 45° direction. The color of the sample area is dark blue, yet the color of the surrounding area is bright red. In Fig. 5(g), the collecting polarization has been rotated to the orthogonal direction. It follows that the sample area becomes bright red, whereas the surrounding area turns to deep blue. Therefore, Figs. 5(f) and 5(g) confirm that this LSS indeed converts the power of the incident light to the orthogonal polarization direction; at the same time, the surrounding area works as a flat mirror with the polarization of reflected light unchanged.

Control the polarization state of light in an extremely limited space has been an important topic in developing integrated optics and on-chip photonics.[37] The work presented here experimentally demonstrates a full-metal broadband stereostructured wave plate. Our stereostructure is basically a continuous metal film and is electrically conductive. So it can be applied as an electrode simultaneously when it plays the role of wave plate. This function may have applications in active opto-electric device[27] and display technology.[28] We believe that this stereostructure provides a unique approach in realizing a broadband wave plate device for manipulating the polarization state of light.

This work has been supported by the grants from the MOST of China (Grant Nos. 2010CB630705 and 2012CB921502), the NSF of China (Grant Nos. 11204127, 11474157, 11034005, and 61475070), the MOE of China (SRFDP No. 20120091120033), and partly by Jiangsu Province (Grant No. BK2012301).

[1]M. Born and E. Wolf, *Principles of Optics*, 7th ed. (Cambridge University Press, Cambridge, 1999).
[2]W. M. Haynes, D. R. Lide, and T. J. Bruno, *CRC Handbook of Chemistry and Physics*, 95th ed. (CRC Press, Boca Raton, FL, USA, 2014).
[3]R. G. Hunsperger, *Integrated Optics: Theory and Technology*, 6th ed. (Springer, New York, 2009).
[4]M. J. Weber, *Handbook of Optical Materials* (CRC Press, Boca Raton, FL, USA, 2002).
[5]N. K. Grady, J. E. Heyes, D. R. Chowdhury, Y. Zeng, M. T. Reiten, A. K. Azad, A. J. Taylor, D. A. R. Dalvit, and H. T. Chen, Science **340**, 1304 (2013).
[6]J. K. Gansel, M. Thiel, M. S. Rill, M. Decker, K. Bade, V. Saile, G. von Freymann, S. Linden, and M. Wegener, Science **325**, 1513 (2009).
[7]S. C. Jiang, X. Xiong, P. Sarriugarte, S. W. Jiang, X. B. Yin, Y. Wang, R. W. Peng, D. Wu, R. Hillenbrand, X. Zhang, and M. Wang, Phys. Rev. B **88**, 161104(R) (2013).
[8]C. Wu, H. Q. Li, Y. Xing, L. Fang, H. Chen, and C. T. Chan, Phys. Rev. Lett. **107**, 177401 (2011).
[9]Y. Zhao, M. A. Belkin, and A. Alu, Nat. Commun. **3**, 870 (2012).
[10]W. Wang, Y. L. Lu, R. J. Knize, K. Reinhardt, and S. C. Chen, Opt. Express **17**, 7361 (2009).
[11]Z. Y. Yang, M. Zhao, P. X. Lu, and Y. F. Lu, Opt. Lett. **35**, 2588 (2010).
[12]X. Xiong, S.-C. Jiang, Y.-H. Hu, J.-M. Zhao, Y.-J. Feng, R.-W. Peng, and M. Wang, AIP Adv. **2**, 041413 (2012).
[13]X. Xiong, W. H. Sun, Y. J. Bao, M. Wang, R. W. Peng, C. Sun, X. Lu, J. Shao, Z. F. Li, and N. B. Ming, Phys. Rev. B **81**, 075119 (2010).
[14]J. M. Hao, Y. Yuan, L. X. Ran, T. Jiang, J. A. Kong, C. T. Chan, and L. Zhou, Phys. Rev. Lett. **99**, 063908 (2007).
[15]N. Liu, H. Liu, S. N. Zhu, and H. Giessen, Nat. Photonics **3**, 157 (2009).
[16]H. Liu, D. A. Genov, D. M. Wu, Y. M. Liu, Z. W. Liu, C. Sun, S. N. Zhu, and X. Zhang, Phys. Rev. B **76**, 073101 (2007).
[17]Z. Wei, Y. Cao, Y. Fan, X. Yu, and H. Li, Appl. Phys. Lett. **99**, 221907 (2011).
[18]K. Aydin, V. E. Ferry, R. M. Briggs, and H. A. Atwater, Nat. Commun. **2**, 517 (2011).
[19]R. H. Fan, L. H. Zhu, R. W. Peng, X. R. Huang, D. X. Qi, X. P. Ren, Q. Hu, and M. Wang, Phys. Rev. B **87**, 195444 (2013).
[20]D. R. Chowdhury, R. Singh, M. Reiten, H. T. Chen, A. J. Taylor, J. F. O'Hara, and A. K. Azad, Opt. Express **19**, 15817 (2011).
[21]A. Pors and S. I. Bozhevolnyi, Opt. Express **21**, 2942 (2013).
[22]N. H. Shen, M. Massaouti, M. Gokkavas, J. M. Manceau, E. Ozbay, M. Kafesaki, T. Koschny, S. Tzortzakis, and C. M. Soukoulis, Phys. Rev. Lett. **106**, 037403 (2011).
[23]Y. X. Cui, K. H. Fung, J. Xu, H. J. Ma, Y. Jin, S. L. He, and N. X. Fang, Nano Lett. **12**, 1443 (2012).
[24]F. Ding, Y. X. Cui, X. C. Ge, Y. Jin, and S. L. He, Appl. Phys. Lett. **100**, 103506 (2012).
[25]J. Grant, Y. Ma, S. Saha, A. Khalid, and D. R. S. Cumming, Opt. Lett. **36**, 3476 (2011).
[26]S. C. Jiang, X. Xiong, Y.-S. Hu, Y.-H. Hu, G.-B. Ma, R.-W. Peng, C. Sun, and M. Wang, Phys. Rev. X **4**, 021026 (2014).
[27]H. T. Chen, W. J. Padilla, J. M. O. Zide, A. C. Gossard, A. J. Taylor, and R. D. Averitt, Nature **444**, 597 (2006).
[28]W. A. MacDonald, J. Mater. Chem. **14**, 4 (2004).
[29]S. Kawata, H. B. Sun, T. Tanaka, and K. Takada, Nature **412**, 697 (2001).
[30]X. Xiong, Z.-H. Xue, C. Meng, S.-C. Jiang, Y.-H. Hu, R.-W. Peng, and M. Wang, Phys. Rev. B **88**, 115105 (2013).
[31]X. Xiong, S.-C. Jiang, Y.-H. Hu, R.-W. Peng, and M. Wang, Adv. Mater. **25**, 3994 (2013).
[32]N. Liu, L. Langguth, T. Weiss, J. Kastel, M. Fleischhauer, T. Pfau, and H. Giessen, Nat. Mater. **8**, 758 (2009).
[33]G. Dolling, C. Enkrich, M. Wegener, C. M. Soukoulis, and S. Linden, Science **312**, 892 (2006).
[34]M. Schroeder, M. Buelters, C. von Kopylow, and R. B. Bergmann, J. Eur. Opt. Soc. Rapid Publ. **7**, 12027 (2012).
[35]See supplementary material at http://dx.doi.org/10.1063/1.4902405 for the retrieval method of phase differences and the discussion of conjugation relation.
[36]J. M. Hao, Q. J. Ren, Z. H. An, X. Q. Huang, Z. H. Chen, M. Qiu, and L. Zhou, Phys. Rev. A **80**, 023807 (2009).
[37]C. M. Soukoulis and M. Wegener, Nat. Photonics **5**, 523 (2011).